Mon. Not. R. Astron. Soc. **315**, 407–422 (2000)

Quantitative analysis of WC stars: constraints on neon abundances from *ISO*-SWS spectroscopy

Luc Dessart,[1★†] Paul A. Crowther,[1] D. John Hillier,[2] Allan J. Willis,[1] Patrick W. Morris[3,4‡] and Karel A. van der Hucht[4]

[1]*Department of Physics & Astronomy, University College London, Gower St, London*
[2]*Department of Physics & Astronomy, University of Pittsburgh, PA 15260, USA*
[3]*Astronomical Institute 'Anton Pannekoek', University of Amsterdam, 1098 SJ Amsterdam, the Netherlands*
[4]*Space Research Organization Netherlands, Sorbonnelaan 2, 3584 CA Utrecht, the Netherlands*

Accepted 2000 January 24. Received 2000 January 21; in original form 1999 November 23

ABSTRACT

Neon abundances are derived in four Galactic WC stars – γ^2 Vel (WR 11, WC8+O7.5III), HD 156385 (WR 90, WC7), HD 192103 (WR 135, WC8) and WR 146 (WC5+O8) – using mid-infrared fine-structure lines obtained with *ISO*-SWS. Stellar parameters for each star are derived using the non-local thermodynamic equilibrium model atmospheric code of Hillier & Miller, together with ultraviolet (*IUE*), optical (INT, AAT) and infrared (UKIRT, *ISO*) spectroscopy. In the case of γ^2 Vel, we adopt very recent results from De Marco et al., who followed an identical approach.

ISO-SWS data sets reveal the [Ne III] 15.5-μm line in each of our targets, while [Ne II] 12.8 μm, [S IV] 10.5 μm and [S III] 18.7 μm are observed solely in γ^2 Vel. Using a method updated from Barlow et al. to account for clumped winds, we derive $\mathrm{Ne/He} = (3\text{–}4) \times 10^{-3}$ by number, plus $\mathrm{S/He} = 6 \times 10^{-5}$ for γ^2 Vel. Neon is highly enriched, such that Ne/S in γ^2 Vel is eight times higher than cosmic values. However, observed Ne/He ratios are a factor of 2 lower than predictions of current evolutionary models of massive stars. An imprecise mass loss and distance were responsible for the much greater discrepancy in neon content identified by Barlow et al.

Our sample of WC5–8 stars span a narrow range in T_* (=55–71 kK), with no trend towards higher temperature at earlier spectral type, supporting earlier results for a larger sample by Koesterke & Hamann. Stellar luminosities range from 100 000 to 500 000 $\mathrm{L_\odot}$, while $10^{-5.1} \leqslant \dot{M}/(\mathrm{M_\odot\ yr^{-1}}) \leqslant 10^{-4.5}$, adopting clumped winds, in which volume filling factors are 10 per cent. In all cases, wind performance numbers are less than 10, significantly lower than recent estimates. Carbon abundances span $0.08 \leqslant \mathrm{C/He} \leqslant 0.25$ by number, while oxygen abundances remain poorly constrained.

Key words: stars: abundances – stars: evolution – stars: fundamental parameters – stars: Wolf–Rayet – infrared: stars.

1 INTRODUCTION

Understanding the physics of massive ($M_{\mathrm{init}} \gtrsim 25\,\mathrm{M_\odot}$) stars, their atmospheres, radiation and evolution is important for many aspects of astrophysics, since their powerful winds affect the energy and momentum balance of the interstellar medium (ISM). In particular, Wolf–Rayet (WR) stars provide crucial tests of nuclear reaction chains.

However, quantitative analysis of such stars represents a formidable challenge. The assumptions of plane-parallel geometry and local thermodynamic equilibrium (LTE), which are often adopted for lower-luminosity stars, are inadequate. Nevertheless, the properties of a large sample of carbon sequence (WC-type) WR stars have now been quantitatively derived using detailed models, accounting for non-LTE effects, spherical geometry and an expanding atmosphere (Howarth & Schmutz 1992; Koesterke & Hamann 1995). However, recent studies have demonstrated that

★ E-mail: ldessart@phy.ulaval.ca (LD); pmorris@ipac.caltech.edu (PWP)
† Present address: Département de Physique, Université Laval and Observatoire du Mont Mégantic, Québec, QC G1K 7P4, Canada.
‡ Present address: SIRTF Science Center/IPAC, California Institute of Technology, M/S 100–22, 1200 E. California Blvd, Pasadena, CA 91125, USA.

clumping (Moffat et al. 1988; Hillier 1991, 1996; Schmutz 1997) and line blanketing (Schmutz 1997; Hillier & Miller 1998) may have a significant effect on the derived physical properties of WR stars.

Overall, evolutionary predictions for massive stars (e.g. Meynet et al. 1994) are in good agreement with the observed properties of Wolf–Rayet stars. van der Hucht & Olnon (1985) derived a Ne/He ratio for γ^2 Vel (WR 11, HD 68273, WC8+O7.5) from *IRAS* space-based observations, which was found to be in good agreement with expectations. However, Barlow, Roche & Aitken (1988, hereafter BRA88) identified a numerical flaw in these calculations and added new ground-based observations to reveal $\mathrm{Ne/He} = 1.0 \pm 0.35 \times 10^{-3}$, a factor of 6 lower than predicted. Is this discrepancy due to failure of evolutionary models, peculiarities of the γ^2 Vel binary system, or incorrect assumptions for the stellar properties of the WC8 star? The combination of Short Wavelength Spectrometer (SWS), *Infrared Space Observatory* (*ISO*) observations of a larger sample of WC stars, plus recent progress in quantitative modelling of WR stars, should provide a definitive answer to this question.

Recent space-based spectroscopy of WR 11, obtained with *ISO*, was presented by van der Hucht et al. (1996), who quoted excellent agreement of the fine-structure neon line fluxes with observations used by BRA88. Morris et al. (1998) subsequently re-estimated Ne/He using contemporary information on the stellar distance (van der Hucht et al. 1997; Schaerer, Schmutz & Grenon 1997) and mass-loss rate (Stevens et al. 1996) of WR 11, which revealed a considerable neon enrichment. Willis et al. (1997, hereafter Paper I) also used *ISO*-SWS to observe WR 146, another WC+O binary, again revealing significantly enriched neon. Recently, Morris et al. (2000) analysed *ISO*-SWS observations of WR 147 (WN8+OB), revealing neon, sulphur and calcium abundances in good agreement with cosmic values, as expected by evolutionary models.

In this paper, we supplement results from Paper I with other WC stars for which *ISO*-SWS observations are available – HD 156385 (WR 90, WC7) and HD 192103 (WR 135, WC8). We also reanalyse WR 146 (WC5+O8) using more sophisticated analysis techniques and in the light of other observational evidence (Niemela et al. 1998; Dougherty, Williams & Pollacco 2000). A neon abundance is also rederived for WR 11, following recent spectroscopic results from De Marco et al. (2000).

The outline of the present work is as follows. New UV, optical and IR observations of our programme stars are presented in Section 2, with basic properties discussed in Section 3. The spectroscopic technique is introduced in Section 4, and applied in Section 5. Our spectroscopic results are discussed in Section 6, with neon and sulphur abundances derived in Section 7. Finally, conclusions are reached in Section 8.

2 OBSERVATIONS

The programme Galactic WC stars are listed in Table 1 where we give the various catalogue names and our adopted spectral types, following Smith, Shara & Moffat (1990) and Crowther, De Marco & Barlow (1998). We will refer to our programme stars by their WR catalogue number (van der Hucht et al. 1981). Wind velocities are taken from UV resonance line measurements (Prinja, Barlow & Howarth 1990; St Louis, Willis & Stevens 1993), except for WR 146 for which a terminal velocity was obtained in Paper I from *ISO*-SWS spectroscopy. In this section, we discuss the ground-based (AAT, INT, ESO) and space-based (*ISO*, *IUE*) observations, the journal of which is presented in Table 2.

Table 1. Programme Galactic WC stars. Spectral types are obtained from Crowther et al. (1998), which follows Smith et al. (1990) except that revised WCE criteria are adopted.

WR	HD	Other	v_∞ (km s^{-1})	Ref.	Spectral type
11	68273	γ^2 Vel	1550	c	WC8+O7.5III
90	156385		2045	a	WC7
135	192103	V1042 Cyg	1405	a	WC8
146		HM19–3	2700	b	WC5+O8

Wind velocities are taken from: (a) Prinja et al. (1990); (b) Willis et al. (1997); (c) St Louis et al. (1993).

Table 2. Journal of optical and IR spectroscopic observations. All SWS observations were obtained with the AOT06 scan.

WR	Epoch	Telescope inst.	Wavelength range (μm)	Exposure time (s)
11	1996 May 17	*ISO*-SWS	2.38–45.2	7876
90	1998 Mar 9	AAT-RGO	0.50–1.03	5
	1997 Feb 16	*ISO*-SWS	2.60–19.6	10068
135	1991 Sep	INT-IDS	0.38–0.73	24
	1994 Aug 20	UKIRT-CGS4	1.03–1.13	64
	1994 Aug 19–21	UKIRT-CGS4	1.61–2.21	576
	1994 Aug 21	UKIRT-CGS4	2.30–2.51	128
	1996 Nov 11	*ISO*-SWS	2.38–45.2	6538
146	1996 Jul 21	INT-IDS	0.36–0.68	800
	1994 Aug 19	UKIRT-CGS4	1.03–1.13	64
	1994 Aug 20	UKIRT-CGS4	1.23–1.33	64
	1994 Aug 19–21	UKIRT-CGS4	1.61–2.21	224
	1994 Aug 21	UKIRT-CGS4	2.30–2.51	64
	1996 May 12	*ISO*-SWS	2.60–19.6	16922

2.1 Ultraviolet spectroscopy

Our UV data set was obtained solely from the *International Ultraviolet Explorer* (*IUE*) archive. Available high-dispersion (HIRES), large-aperture, short- (SWP) and long-wavelength (LWP, LWR) observations of WR 90 and WR 135 were combined to provide high signal-to-noise ratio (S/N) data sets (St Louis 1990). Absolute flux calibration was achieved following the calibration curve obtained by Howarth & Phillips (1986). Agreement between our final HIRES data sets and archival low-resolution (LORES) observations was found to be excellent.

Willis et al. (1986) have discussed the UV spectral morphology of WC stars, including WR 90 and WR 135. The principal spectral features for both stars are Si IV λλ1393–1407, C IV λλ1548–1551, He II λ1640 and C III λ2297. A forest of Fe V–VI lines are present in both stars, with Fe IV also prominent in WR 135.

2.2 Optical spectroscopy

Previously unpublished spectroscopic observations of WR 90 and WR 135 were obtained at the 2.5-m Isaac Newton Telescope (INT) and 3.9-m Anglo Australian Telescope (AAT). The INT data set was obtained with the IDS, 500-mm camera, and GEC CCD during 1991 September, while the AAT data set was obtained with

the RGO spectrograph, 25-cm camera, and an MIT/LL CCD during 1998 March. Each data set was obtained using charge-coupled devices (CCDs) and reduced in a standard manner using software available on Starlink. Spectra were debiased, flat-fielded, optimally extracted, wavelength calibrated, and flux calibrated in the case of the INT data set. Flux calibration was achieved for the AAT observations via scaling to the level of the blue CTIO spectrophotometry taken from Torres-Dodgen & Massey (1988).

Arc spectra provided a measure of the instrumental resolution: 2–3 Å (INT) and 4 Å (AAT). Complete spectral coverage of 3800–7300 Å (INT) and 5000–10 300 Å (AAT) was achieved with, respectively, six and one grating settings. The atmospheric absorption bands were removed using suitable comparison stars.

The optical spectral appearance of WR 146 has previously been discussed in Paper I, while Dougherty et al. (2000) present a new high-quality blue optical observation of that star. The morphologies of WR 90 and WR 135 are relatively similar, dominated by He I–II and C III–IV emission features, except that the emission lines of WR 90 are substantially broader. C III $\lambda\lambda$4747–4751 and C IV $\lambda\lambda$5801–5812 are the two strongest features in each case. Several O III–V features are present around $\lambda\lambda$2950–3150, and λ5592 with C II present at λ4267 for WR 135.

2.3 Near-IR spectroscopy

Our principal near-IR data set was obtained at the 3.8-m UK Infrared Telescope (UKIRT) with the cooled grating spectrograph CGS4, the 300-mm camera, a 75 line mm^{-1} grating and a 62×58 InSb array in 1994 August. Observations of WR 135 and WR 146 were bias-corrected, flat-fielded, extracted and sky-subtracted using CGS4DR (Daly & Beard 1992). Subsequent reductions and analysis were carried out using FIGARO (Shortridge et al. 1999) and DIPSO (Howarth et al. 1998). In order to remove atmospheric features, the observations were divided by an appropriate standard star (whose spectral features were artificially removed) observed at around the same time and similar air mass. In regions of low atmospheric transmission at UKIRT the reliability of line shape and strength must be treated with caution (e.g. the Pα region). The near-IR morphologies of WR 135 and WR 146 have been discussed previously by Eenens, Williams & Wade (1991).

We also utilize intermediate dispersion CCD spectra of WR 135 covering 0.97–1.03 μm, published by Howarth & Schmutz (1992), and obtained at the INT with the Intermediate Dispersion Spectrograph (IDS) and a GEC CCD in 1990 October. Although Howarth & Schmutz (1992) obtained observations of the He I λ10 830+Pγ line, we prefer to use our new, lower-resolution UKIRT observations of this feature. (The sharp fall in efficiency of the GEC CCD longward of Pγ leads to an ill-defined continuum.) We attempt an approximate flux calibration for these data, by setting the local continuum via interpolation of the observed 0.7-μm (INT) and 1.03-μm (UKIRT) flux levels.

2.4 Mid-IR spectroscopy

New mid-IR data of WR 90 and WR 146 were obtained as part of Guest Observer programme, AJWWOLF (P. I. Willis), with the Short Wavelength Spectrograph (SWS; de Graauw et al. 1996) on-board the ESA *Infrared Space Observatory* (Kessler et al. 1996). Observations of HD 117297 (WR 53), HD 164270 (WR 103) and HD 165763 (WR 111) from the AJWWOLF programme were of insufficient quality to provide mid-IR line flux measurements, and so these were excluded from the present study. Consequently, we have included SWS observations of WR 11 and WR 135 from the Guaranteed Time programme WRSTARS (P. I. van der Hucht). In all cases the SWS AOT6 observing mode was used to achieve full grating resolution, $\lambda/\Delta\lambda \simeq$ 1300–2500. The continuous wavelength coverage was 2.60–19.6 μm for data sets from the AJWWOLF programme, and 2.38–45.0 μm for WR 135 and WR 11.

Data of detector 'bands' 1 and 2 respectively cover wavelengths of 2.38–4.08 μm using 12 In:Sb detectors and 4.00–12.05 μm with 12 Si:Ga detectors, employing entrance slits that give an effective aperture area of 14×20 arcsec on the sky. Band 3A to 3D data cover 12.0–27.6 μm using 12 Si:As detectors, with sky coverage of 14×27 arcsec. Finally, band 3E and 4 data cover 27.5–45.0 μm using 12 Ge:Be detectors, with sky coverage of 20×33 arcsec.

The total integration time was set to allow one complete scan over the wavelengths selected within each 'AOT band', defined by the permissible combinations of detector band, aperture and spectral order (cf. de Graauw et al. 1996). The observation time includes dark current measurements, and a monitor of photometric drift for the detectors of bands 2 and 3. A drift measurement is not normally made for the relatively stable In:Sb detectors.

The data processing of the SWS data for WR 146 was discussed in Paper I, with WR 11, WR 90 and WR 135 reduced in a similar manner. The stellar spectrum of WR 11 will be discussed elsewhere (Morris et al., in preparation), with solely mid-IR fine-structure line fluxes measured here.

3 INTERSTELLAR REDDENING AND DISTANCES

In this section, interstellar reddenings and distances to the programme stars are discussed. Pre-empting results from Section 4, reddenings are directly obtained from comparing theoretical synthetic spectra with dereddened observations. Distances follow from either cluster/association membership or assumed absolute magnitudes. Table 3 provides a summary of the derived reddenings and distances for our sample of stars. A comparison with reddenings from the recent literature shows good agreement. The distances to WR 135 (Cyg OB3 member) and WR 11 (*Hipparcos*) are known with confidence, while those adopted here for WR 90 and WR 146 deserve comment.

3.1 WR 90

WR 90 is not a member of an association or cluster. We therefore

Table 3. Summary of photometry, reddenings and distances for programme stars, including comparisons with reddenings from the literature (lit.). Observed magnitudes correspond to the systemic value for binary systems, and include the Schmutz & Vacca (1991) corrections to Smith (1968) photometry (*).

WR	v^{sys} (mag)	Ref.	E_{B-V}(lit.) (mag)	R	Ref.	M_v^{WC} (mag)	d (kpc)	Ref.
11	1.70*	a	0.04 (0.03)	3.1	e	−3.7	0.26	h
90	7.41*	a	0.38 (0.44)	3.1	d	−4.7	1.55	e
135	8.51	b	0.37 (0.35)	3.1	a	−4.3	2.09	f
146	13.91	c	2.87 (2.80)	2.9	c	−5.3	1.40	g

Refs: (a) Smith (1968); (b) Massey (1984); (c) Paper I; (d) Morris et al. (1993); (e) Schaerer et al. (1997); (f) Lundström & Stenholm (1984); (g) Dougherty et al. (2000); (h) van der Hucht et al. (1997).

estimated its distance based on the mean absolute visual magnitude of other Galactic WC7 stars. Unfortunately, all five WC7 stars that are members of associations/clusters are within binary systems (Lundström & Stenholm 1984). We restricted the sample to those for which reliable reddenings were known (HD 97152 = WR 42, HD 152270 = WR 79 and HD 192641 = WR 137) from Morris et al. (1993). An absolute visual magnitude of $M_{\rm v} = -4.7$ mag ($\sigma = 0.8$) was obtained for the WC7 components by comparing their emission line strengths with WR 90 (specifically C III–IV λ4650, C IV λ5804). Our estimate is in good agreement with van der Hucht et al. (1988) and Smith et al. (1990), who derived $M_{\rm v} = -4.8$ mag. Pre-empting results from Section 5 we derive $E_{B-V} = 0.38$ mag, so that the uncertainty in the calibration and reddening (± 0.02 mag) implies $d = 1.5^{+0.5}_{-0.4}$ kpc.

3.2 WR 146

Dougherty et al. (1996) used IR and millimetre photometry to estimate a distance of 1.2 ± 0.3 kpc towards WR 146. Radio observations revealed two separate components, namely the (thermal) WC emission plus the (non-thermal) bow shock emission between the two winds.

Meanwhile, a lower distance of 0.75 ± 0.15 kpc was derived in Paper I, using the mean $M_{\rm v}$ for a WCE star (Smith et al. 1990), plus an assumed spectral type of O8.5V for the companion. Subsequently, Niemela et al. (1998) used WFPC2 aboard the *Hubble Space Telescope* (*HST*) to measure the individual *UBV* magnitudes of the WC and OB components of WR 146. They derived $V = 13.64$ mag for the WC star, 0.24 mag brighter than the OB component. In contrast, a difference of 0.8 mag was assumed in Paper I.

The combined *HST* and radio data sets indicate that the OB companion possesses a powerful stellar wind, with a giant or supergiant luminosity class. Recent optical spectroscopy supports a supergiant O8 classification (Dougherty et al. 2000). As discussed by Dougherty et al., a large distance to this system would result if the absolute magnitude of the companion was typical of late O supergiants (Conti & Alschuler 1971). Instead, we adopt the distance of 1.4 kpc, as derived by Dougherty et al. At this distance, WR 146 would be a foreground object to Cyg OB2 (Lundström & Stenholm 1984; Torres-Dodgen, Carroll & Tapia 1991).

We derived $E_{B-V} = 2.87$ mag and $R = 2.9$ using the optical–IR reddening law of Steenman & Thé (1989, 1991). This provided a superior comparison between theoretical predictions and dereddened observations than with either the Howarth (1983) or Cardelli, Clayton & Mathis (1989) laws. Therefore, $M_{\rm v} = -5.3$ mag for the WCE component, by far in excess of 'typical' WCE stars (Smith et al. 1990).

4 MODELLING TECHNIQUE

Before discussing the fine analysis of each programme star, we introduce the spectroscopic technique followed here. We use the non-LTE code of Hillier & Miller (1998), which iteratively solves the transfer equation in the comoving frame subject to statistical and radiative equilibria in an expanding, spherically symmetric and steady-state atmosphere. Relative to earlier versions of this code (Hillier 1987, 1990), two major enhancements have been incorporated, of particular relevance to WC-type stars, namely (i) line blanketing and (ii) clumping. Specific details of the techniques used are provided by Hillier & Miller (1998, 1999), with only a brief overview given here.

As discussed by Hillier & Miller (1998, 1999), extremely complex atomic models are necessary for the quantitative analysis of WC stars, a computationally demanding requirement. Consequently, we make use of the technique of 'super-levels', in which several atomic levels of similar energies and properties are combined into a single one, a super level, with the populations of the super level calculated in the rate equations. Populations of individual atomic levels are then calculated by assuming that it has the same departure coefficient as the corresponding super level to which it belongs. In this way, extremely complex atoms of helium, carbon, oxygen and iron can be considered. In Table 4 a total of 1299 full ($N_{\rm F}$) atomic levels are combined to produce just 440 super levels ($N_{\rm S}$). The number of iron transitions is limited by $gf \leqslant 10^{-4}$, so that a total of 20 007 transitions are included. In addition to the specific models discussed here, we have also considered cases with expanded atomic data sets and ionization stages (e.g. Fe III), for which the differences in emergent synthetic spectrum were negligible.

Oscillator strengths, collision and photoionization cross-sections are taken from a wide variety of sources (Table 4). The OPACITY project (Seaton 1987, 1995) formed the basis of most radiative rates, supplemented by calculations for CNO by Nussbaumer & Storey (1983, 1984) and Storey (unpublished), and for iron by Becker & Butler (1992, 1995a,b) and Butler (unpublished).

The stellar radius (R_*) is defined as the inner boundary of the model atmosphere and is located at Rosseland optical depth of 10 with the stellar temperature (T_*) defined by the usual

Table 4. Summary of the WC model atoms, and source of atomic data sets. $N_{\rm F}$ is the number of full levels, $N_{\rm S}$ the number of super levels and $N_{\rm trans}$ the corresponding number of transitions. The last column refers to the upper level of a given ion included in our treatment.

Species	$N_{\rm F}$	$N_{\rm S}$	$N_{\rm trans}$	Ref.	Details
He I	39	27	315	a	$n \leqslant 14$
He II	30	13	435	b	$n \leqslant 30$
He III	1	1			
C II	88	39	791	c,d	$nl \leqslant$ 2p3d ^{4}D$^{\rm o}$
C III	243	99	5513	e,f	$nl \leqslant$ 2p4d ^{1}D$^{\rm o}$
C IV	64	49	1446	g	$n \leqslant 30$
C V	1	1			
O II	3	3	3	e,h	$nl \leqslant$ 2p^3 ^{2}P$^{\rm o}$
O III	50	50	213	e,i	$nl \leqslant$ 2p4f ^{1}D
O IV	72	30	835	e,j	$nl \leqslant$ 2p3p$''$ ^{2}P$^{\rm o}$
O V	91	31	748	e,k	$nl \leqslant$ 2p4p ^{3}P
O VI	19	13	72	g	$n \leqslant 5$
O VII	1	1			
Si IV	28	17	129	h	$n \leqslant 6$
Si V	1	1			
Fe IV	280	21	5055	l	$nl \leqslant$ 3d^4(^{1}G)4p ^{2}P$^{\rm o}$
Fe V	182	19	2517	m	$nl \leqslant$ 3d^3(^{2}D)4p ^{1}P$^{\rm o}$
Fe VI	80	10	722	n	$nl \leqslant$ 3d^2(^{1}S)4p ^{2}P$^{\rm o}$
Fe VII	153	14	1213	o	$nl \leqslant$ 3p^5(^{2}P)3d^3(b^{2}D) ^{1}P$^{\rm o}$
Fe VIII	1	1			
	1299	440	20007		

Refs: (a) Fernley, Seaton & Taylor (1987); (b) Wiese, Smith & Glennon (1966); (c) Yu Yan, Taylor & Seaton (1987); (d) Yu Yan & Seaton (1987); (e) Nussbaumer & Storey (1983, 1984); (f) P. J. Storey (unpublished); (g) Peach, Saraph & Seaton (1988); (h) Seaton (1995); (i) Luo et al. (1989); (j) Luo & Pradhan (1989); (k) Tully, Seaton & Berrington (1990); (l) Becker & Butler (1995b); (m) Becker & Butler (1992); (n) Becker & Butler (1995a); (o) K. Butler (unpublished).

Stefan–Boltzmann relation. Similarly, $T_{2/3}$ relates to the radius ($R_{2/3}$) at which the Rosseland optical depth equals 2/3.

Although the majority of spectral analyses of WR stars have adopted a standard $\beta = 1$ velocity law, there is both observational and theoretical evidence for a more slowly accelerating outflow (e.g. Schmutz 1997; Lepine & Moffat 1999). Consequently, we adopt a form for the velocity law (equation 8 from Hillier & Miller 1999) such that two exponents are considered, with the result that acceleration is modest at small radii, but continues to large distances, i.e.

$$v(r) = \frac{v_0 + (v_\infty - v_{\rm ext} - v_0)(1 - R_*/r)^{\beta_1} + v_{\rm ext}(1 - R_*/r)^{\beta_2}}{1 + (v_0/v_{\rm core})\exp[(R_* - r)/h_{\rm eff}]}.$$

Here $v_{\rm ext}$ is an intermediate terminal velocity, $v_{\rm core}$ is the core velocity (typically a few $\rm km\,s^{-1}$), v_0 is the photospheric velocity (typically $100.0\,\rm km\,s^{-1}$), v_∞ is the final wind velocity and $h_{\rm eff}$ is the scaleheight ($\sim 0.01 R_*$). For all models, we take $\beta_1 = 1$ and $\beta_2 = 50$ as in Hillier & Miller (1999).

There is now overwhelming evidence for the clumped nature of WR stars (e.g. Moffat et al. 1988; Moffat 1999), so we have adopted a simple filling factor approach. We assume that the wind is clumped with a volume filling factor, f, and that there is no interclump material. Since radiation instabilities are not expected to be important in the inner wind, we parametrize the filling factor so that it approaches unity at small velocities. Clumped and non-clumped spectra are very similar, except that line profiles are slightly narrower with weaker electron scattering wings in the former. Although non-clumped models can be easily rejected, because of the severe line blending in WC winds $\dot{M}/\sqrt{f}$ is derived by our spectroscopic analysis, rather than $\dot{M}$ and f. Also, this formulation introduces a revision of the BRA88 analytical formula, which will be addressed in Section 7.

5 SPECTROSCOPIC ANALYSIS OF INDIVIDUAL STARS

In this section, we discuss the analysis of our programme WC stars. Stellar parameters – T_*, $\log(L/{\rm L}_\odot)$, $\dot{M}/\sqrt{f}$, C/He, O/He – were adjusted until the observed ionization balance, line strengths and dereddened optical continuum flux distribution were reproduced. Because of the substantial effect that differing mass-loss rates, temperatures and elemental abundances have on the emergent spectrum, this was an iterative process, in which initial model parameters were adopted from the literature if available (e.g. Morris et al. 1993; Koesterke & Hamann 1995). Terminal wind velocities are tabulated in Table 1.

The wind ionization balance was ideally selected on the basis of isolated optical lines from adjacent ionization stages of carbon and/or helium. In practice this was difficult to achieve because of the severe blending in WC winds. The low wind velocity of WR 135 allowed He I λ5876 and He II λ5412 to be used as ionization balance constraints. In other cases, the wind ionization balance was selected on the basis of carbon diagnostics. Unfortunately, from all the possible WC diagnostics, the usual classification lines C III λ5696/C IV λ5804 are difficult to match, being so sensitive to minor stellar parameter changes. Consequently alternative diagnostics were sought. For WR 90, our primary diagnostics were C III λ8500/C IV λ7736, since these suffered from negligible contamination and are predicted by the model to vary smoothly across the temperature space. In the case of WR 146 this spectral region, as well as lines of low ionization, were not available. We selected He II λ5412/He I λ10 830 and C III λ6740/C IV 1.74 μm as our primary ionization diagnostics.

Our experience with a variety of stellar models led us to select the strong ultraviolet P-Cygni profiles of carbon (C III $\lambda\lambda$1909, 2297) as our principal mass-loss diagnostics. A major limitation with C IV λ1550 was that different mass-loss rates also affected nearby Fe lines, which strongly modulated the predicted strength of the emergent P-Cygni profile. Since ultraviolet observations of WR 146 are unavailable, we relied on He I λ10 830 as the principal mass-loss diagnostic in that case.

As in other recent spectroscopic studies of WC stars, He II λ5412/C IV λ5471 were selected as the diagnostics for C/He determinations since the relative strengths of these features are insensitive to differences of temperature or mass-loss rate. As discussed by Hillier & Miller (1998), this spectral region also contains a number of additional weak features, common to all stars. More problematic is that misleading C/He ratios would be obtained if: (i) a limited number of C IV atomic levels were included; (ii) homogeneous models were adopted in which electron scattering wings were incorrectly predicted.

Test calculations were also performed using recombination theory. Comparisons of C/He with our more sophisticated results for WCE stars was found to be reasonable – we obtain C/He = 0.08 by number for WR 146 in this study, in accord with the value obtained by Eenens & Williams (1992) based on IR recombination lines. WCL stars are more problematic since recombination coefficients for C III are not available. In addition, the fraction of recombined helium is not straightforward to assess in such studies, so that helium abundances could be underestimated.

Oxygen abundances were more difficult to constrain, as already discussed by Hillier & Miller (1999), with the principal diagnostic region spanning $\lambda\lambda$2900–3500. Since this spectral region was absent for WR 146, we adopted C/O = 4 by number, as predicted by current stellar evolutionary models. Note that our neon abundance determination in Section 7 is relatively insensitive to the precise oxygen content. Regarding silicon and iron, we adopt solar abundances since all distances are $\leqslant$2 kpc.

We now proceed to discuss individual stars in detail.

5.1 HD 156385 (WR 90)

The principal data sets for WR 90 comprised HIRES *IUE* ultraviolet spectroscopy and AAT/RGO spectrograph optical observations. Secondary data sets were the blue CTIO spectroscopy from Torres-Dodgen & Massey (1988) and the 2.6–5 μm *ISO* spectroscopy (longer-wavelength data were of insufficient S/N to be used as stellar diagnostics). The combined, UV–optical–IR flux-calibrated data set for WR 90 allowed a well-constrained reddening of $E_{B-V} = 0.38$ mag, in agreement with the determination by Morris et al. (1993) (see Table 3). A distance of 1.55 kpc is implied from our assumed WC7 $M_{\rm v}$ calibration.

The difficulty in identifying the stellar continuum in the rich emission-line spectrum of WC stars makes rectification imprecise, as emphasized byHillier & Miller (1998, 1999). Fig. 1 demonstrates the excellent agreement between the line and continuum distribution of the model spectrum (dotted lines) and observations (solid lines), and includes the true theoretical continuum distribution (dashed lines). The number of line features that are poorly reproduced is small, and includes C III λ5696 (too weak), λ9710 (too strong), plus C IV $\lambda\lambda$1548–1551, Si IV $\lambda\lambda$1393–1402 (both too weak because of Fe absorption) and O VI $\lambda\lambda$3811–3834

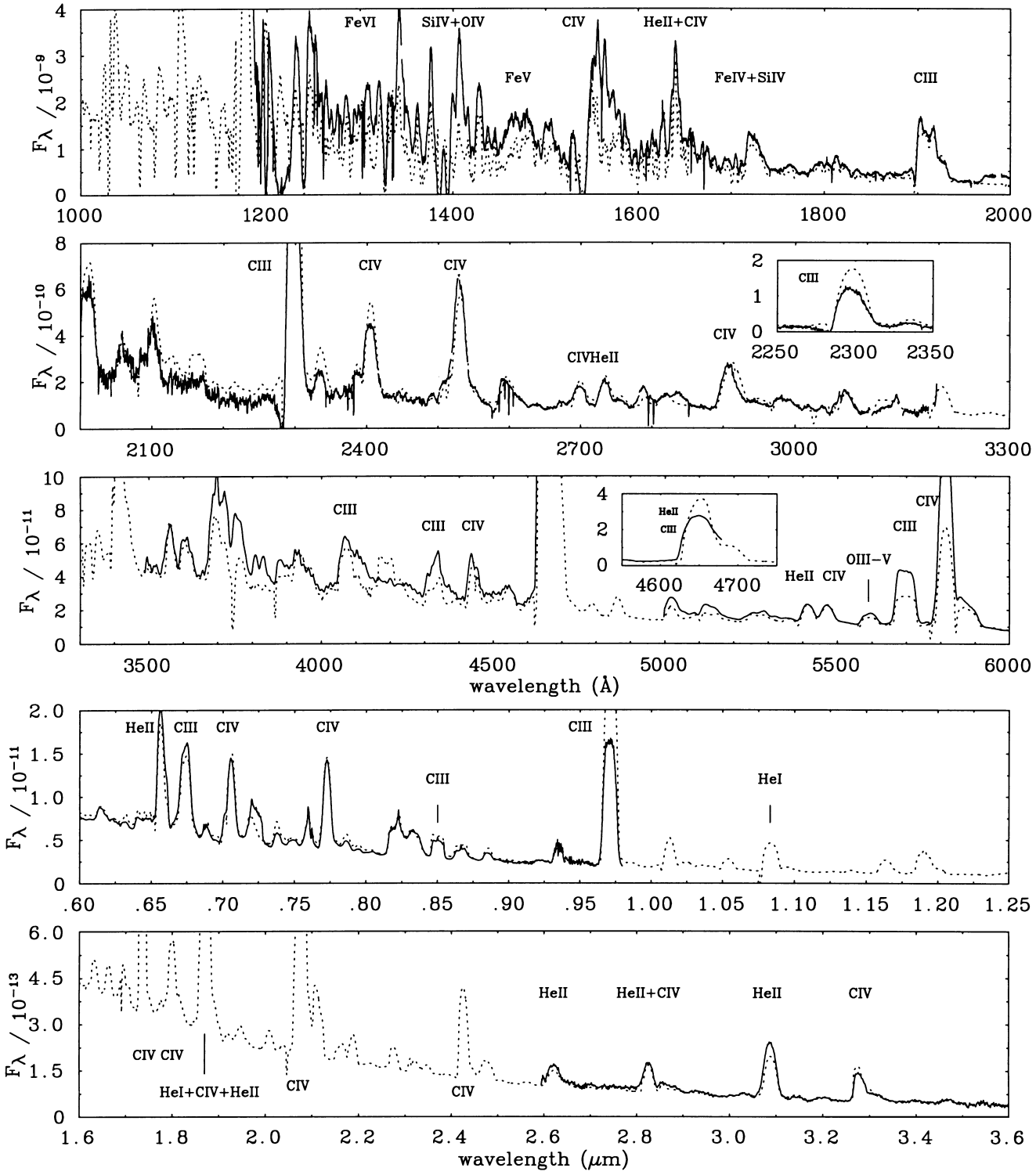

Figure 1. Comparison between the dereddened ($E_{B-V} = 0.38$, $R = 3.1$) spectrophotometry of HD 156385 = WR 90 (WC7) obtained from *IUE*, CTIO, AAT and *ISO* (solid lines), and line-blanketed, clumped model predictions (dotted lines). Stellar parameters are $\dot{M} = 2.5 \times 10^{-5}\,\mathrm{M_\odot\,yr^{-1}}$, $T_* = 71\,\mathrm{kK}$, $\log(L/\mathrm{L_\odot}) = 5.5$, C/He = 0.25 and O/He = 0.03 by number. Flux units are in $\mathrm{erg\,cm^{-2}\,s^{-1}\,\AA^{-1}}$.

(too weak). The use of absolute fluxes appears to give poor results in the line strengths around C III λ2297 since the dereddened and theoretical continua do not exactly match.

Our analysis reveals stellar parameters of $T_* = 71\,000\,\mathrm{K}$, $\log(L/\mathrm{L_\odot}) = 5.5$ and $\dot{M}/\sqrt{f} = 8 \times 10^{-5}\,\mathrm{M_\odot\,yr^{-1}}$. Adopting a volume filling factor of $f = 0.1$ indicates $\log[\dot{M}/(\mathrm{M_\odot\,yr^{-1}})] = -4.6$ and a wind performance number of ~8. Use of C IV λ5471/He II λ5412 revealed C/He = 0.25 ± 0.05 by number. An oxygen abundance of O/He = 0.03 ± 0.01 by number was obtained by matching O IV λλ2916–2926, λλ3063–3072 and λλ3560–3563.

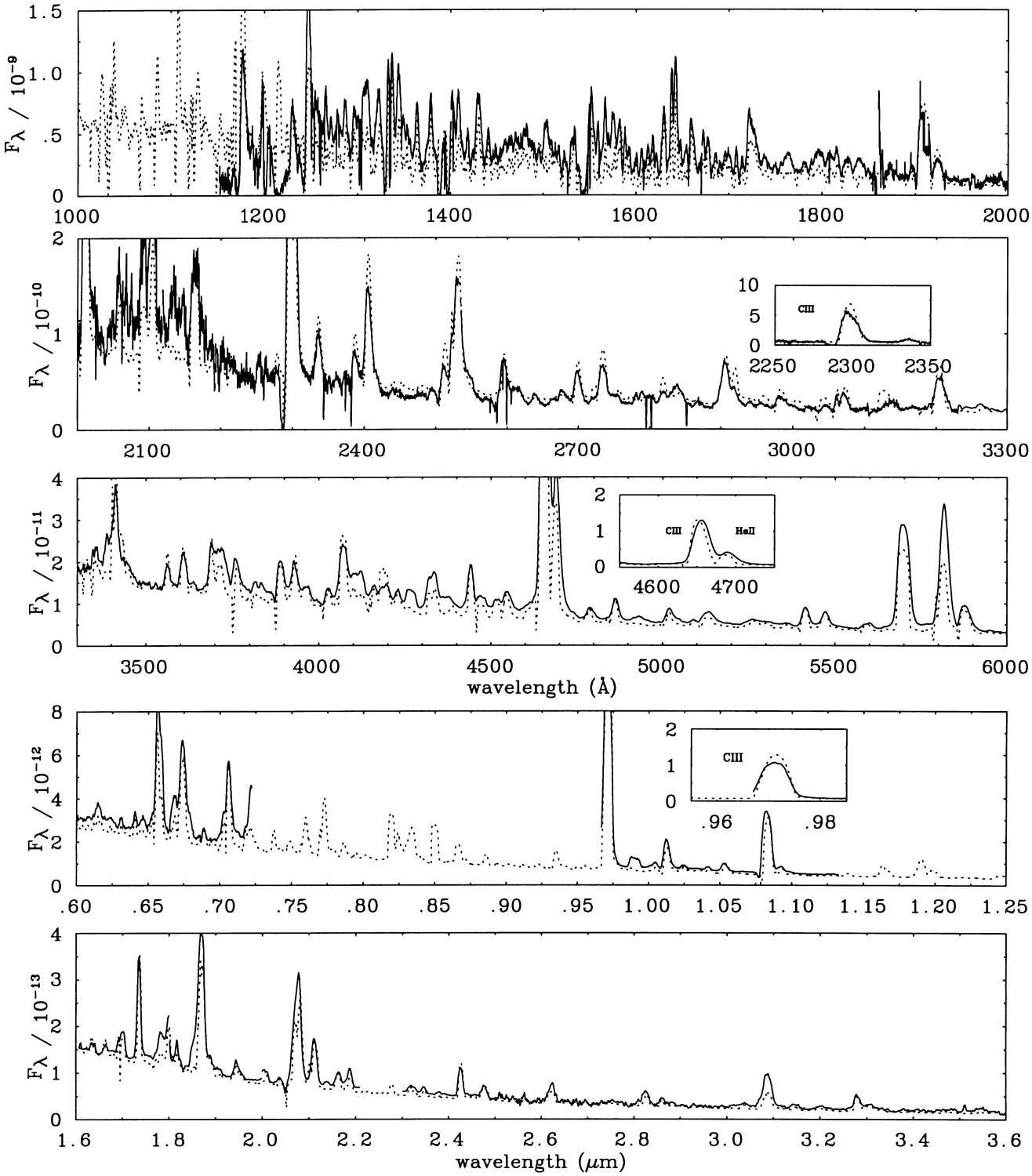

Figure 2. Comparison between the dereddened ($E_{B-V} = 0.37$, $R = 3.1$) spectrophotometry of HD 192103 = WR 135 (WC8) obtained from *IUE*, INT, UKIRT and *ISO* (solid lines) and line-blanketed, clumped model predictions (dotted lines). Stellar parameters are $\dot{M} = 1.3 \times 10^{-5}\,\mathrm{M_\odot\,yr^{-1}}$, $T_* = 63\,\mathrm{kK}$, $\log(L/\mathrm{L_\odot}) = 5.20$, C/He = 0.13 and O/He = 0.03 by number. Flux units are in $\mathrm{erg\,cm^{-2}\,s^{-1}\,\AA^{-1}}$.

5.2 HD 192103 (WR 135)

A substantial observational data set was available for the WR 135 analysis, particularly high-quality UV (HIRES *IUE*), optical (INT), near-IR (INT, UKIRT) and mid-IR (*ISO*) spectrophotometry. An interstellar reddening of $E_{B-V} = 0.37$ was obtained for WR 135, in accord with Smith et al. (1990) (see Table 3), but 0.18 mag lower than the more recent determination of Morris et al. (1993). Membership of Cyg OB3 implied an absolute visual magnitude of $M_\mathrm{v} = -4.3$ mag.

Dereddened spectroscopy of WR 135 (solid lines) is compared to our final synthetic model (dotted lines) in Fig. 2. Agreement is

overall excellent, even for the forest of iron lines in the UV. The relatively low wind velocity of WR 135 permits a greater number of individual diagnostics to be selected, including He II λ4686, He I λ5876, so that the derived properties can be treated with confidence. Indeed, C III λ5696 and C IV λ5804 are fairly well matched in this case. The strong C III spectral features at λλ2297 and 9710 are predicted to be 20–30 per cent too strong. Other notable model deficiencies include underestimating the strength of C II emission at λλ4267, 9900, and O VI λλ3811–3834, with O III λ3130 too strong. As with WR 90, the use of absolute fluxes appears to give poor results in the line strengths around He II λ2530 since the dereddened and theoretical continua do not exactly match. This discrepancy simply reflects the inadequacy of the adopted reddening law, rather than a fundamental flaw with current models.

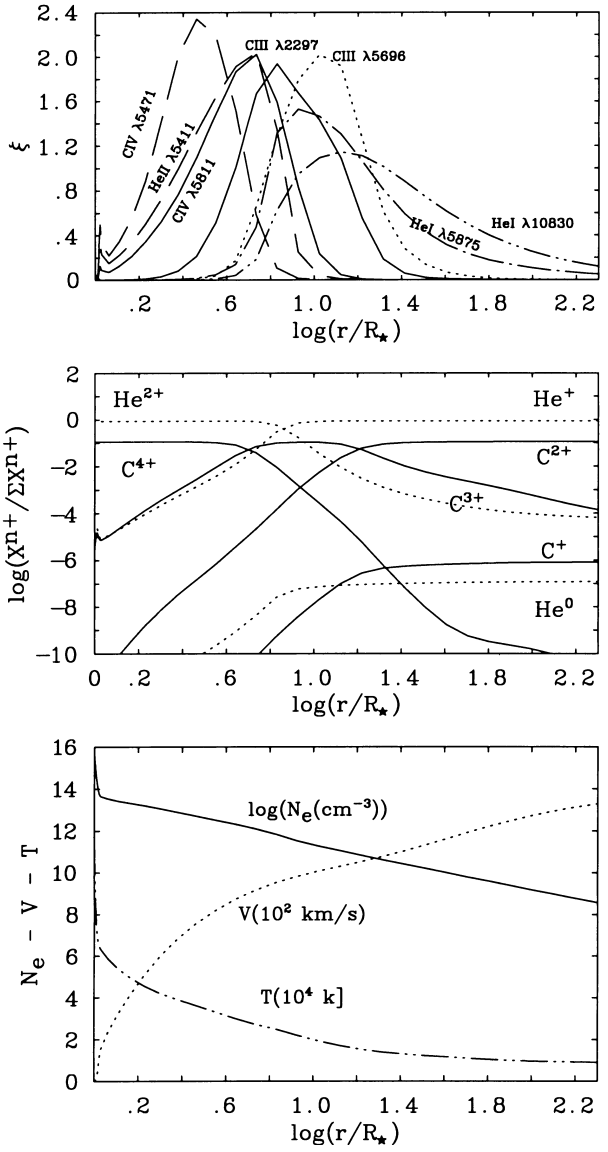

Figure 3. Model predictions for the WC8 star WR 135, analysed in Section 5.2. **Top**: Line formation regions for a selection of lines. The parameter ξ is related to the observed flux emitted in the corresponding line, and defined as in Hillier (1987). The integral of ξ over $\mathrm{d}\log(r/R_*)$ is proportional to the equivalent width. **Middle**: Wind ionization stratification for carbon (solid) and helium (dotted). Note that helium does not recombine to its neutral state in the outer wind. **Bottom**: Radial dependence of electron temperature (kK, dot-dash), density (cm^{-3}, solid) and wind velocity ($\mathrm{km\,s}^{-1}$, dotted).

We obtain the following stellar parameters: $T_* = 63$ kK, $\log(L/\mathrm{L}_\odot) = 5.2$ and $\dot{M}/\sqrt{f} = 3.8 \times 10^{-5}\,\mathrm{M}_\odot\,\mathrm{yr}^{-1}$. Adopting a volume filling factor of $f = 0.1$ indicates $\log[\dot{M}/(\mathrm{M}_\odot\,\mathrm{yr}^{-1})] = -4.9$ and a wind performance number of ∼8. Use of C IV λ5471/He II λ5412 revealed $\mathrm{C/He} = 0.13 \pm 0.03$ by number. Once again, the oxygen abundance is poorly constrained, although $\mathrm{O/He} = 0.03 \pm 0.01$ provides a reasonable match to O IV λλ2916–2926 and 3063–3072, with O III λ3127 too strong.

In Fig. 3, we present the wind structure of the final WR 135 synthetic model, including line formation regions, ionization balance, etc. Similar relations are shown for WR 111 (WC5) in Hillier & Miller (1999).

5.3 WR 146

Our principal observational data sets for WR 146 are identical to those used in Paper I, namely INT (optical), UKIRT (near-IR) and *ISO* (2.6–5 μm because of the low S/N at longer wavelengths). The difference in our approach is to derive stellar and chemical properties solely from spectral synthesis, rather than recombination theory and independent modelling of the continuum. As discussed in Section 3.2, we follow the distance estimate of 1.4 kpc from Dougherty et al. (2000), in the light of new observations from Niemela et al. (1998).

We have included the spectral energy distribution of a O8 supergiant in our synthesis, using that for HD 151804 (O8If) derived by Crowther & Bohannan (1997). The IR free–free excess of this model is somewhat greater than equivalent temperature Kurucz (1991) models, for which the lowest gravity available is $\log g = 4$. Because of the contamination from the late O supergiant, the line spectrum of the WC component of WR 146 is relatively weak, as shown in Fig. 4. The flux level of the O companion, the contribution of which declines with increasing wavelength, is illustrated as a dashed line in Fig. 4. Comparison between dereddened observations and our synthetic spectrum is excellent, with the notable exception of C IV λ5804.

Our final stellar parameters for the WC5 star were $\mathrm{T}_* = 57$ kK, $\log(L/\mathrm{L}_\odot) = 5.7$ and $\dot{M}/\sqrt{f} = 1 \times 10^{-4}\,\mathrm{M}_\odot\,\mathrm{yr}^{-1}$. A filling factor of $f = 0.1$ reproduced the red wing of C III–IV λ4650–He II λ4686. The high wind velocity of WR 146 meant that C IV λ5471/He II λ5412 were blended. Nevertheless, we were able to constrain the carbon content, deriving $\mathrm{C/He} = 0.08 \pm 0.02$ by number, a factor of 2 times lower than that estimated in Paper I from recombination line analysis, but now in accord with Eenens & Williams (1992). Oxygen is extremely difficult to measure in WR 146 since the usual near-UV diagnostics are unavailable, so that $\mathrm{O/He} = 0.02 \pm 0.01$ is adopted.

Finally, should the absolute magnitude of WR 146 be more typical of other WCE stars, namely $M_\mathrm{v} = -3.7$ mag (Smith et al. 1990), what would be the effect on the derived stellar parameters? In this case, our reddening towards WR 146 would imply a distance of 660 pc, such that the companion star would be extremely faint, $M_\mathrm{v} = -3.5$ mag, typical of an early B dwarf. The stellar properties of WR 146 would be unchanged, except that $\log(L/\mathrm{L}_\odot) = 5.0$, and $\dot{M}/\sqrt{f} = 3.3 \times 10^{-5}\,\mathrm{M}_\odot\,\mathrm{yr}^{-1}$. In this case it would be difficult to reconcile these properties with the *HST*/radio observations of WR 146 (Dougherty et al. 1996; Niemela et al. 1998).

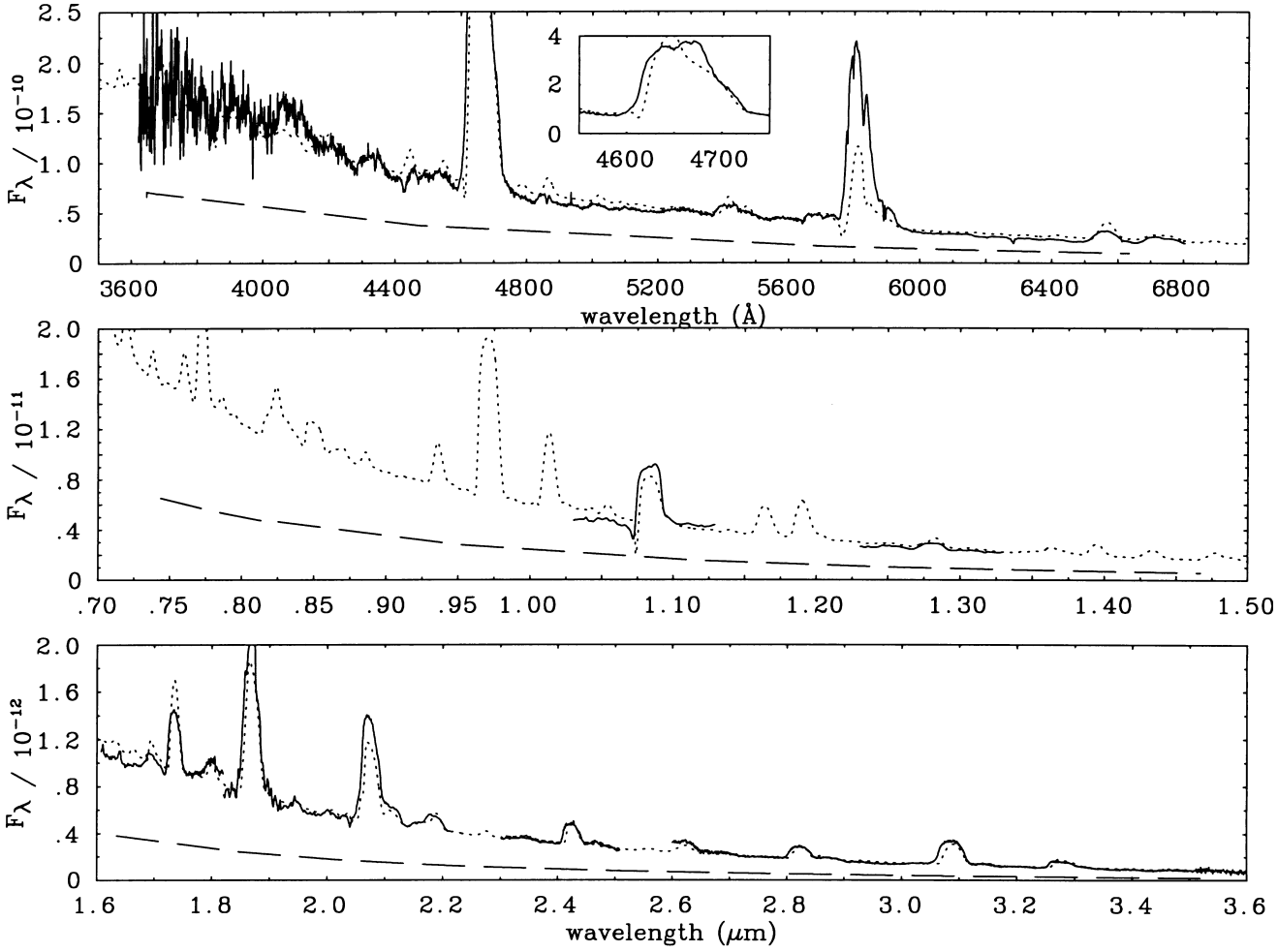

Figure 4. Comparison between the dereddened ($E_{B-V} = 2.87$ mag, $R = 2.9$) spectrophotometry of WR 146 (WC5+OB) obtained from INT, UKIRT and *ISO* (solid lines) and line-blanketed, clumped model predictions (dotted lines). The contribution of the late O companion is taken into consideration, using model calculations by Crowther & Bohannan (1997) – its continuum distribution is indicated with dashed lines. WC stellar parameters are $\dot{M} = 3.3 \times 10^{-5}\,\mathrm{M_\odot\,yr^{-1}}$, $T_* = 57$ kK, $\log(L/\mathrm{L_\odot}) = 5.7$, C/He = 0.08 and O/He = 0.02 by number. Flux units are in $\mathrm{erg\,cm^{-2}\,s^{-1}\,\AA^{-1}}$.

Table 5. Derived stellar properties for programme WC stars, including results obtained by De Marco et al. (2000) for WR 11 and Hillier & Miller (1999) for WR 111 for comparison.

WR	Spectral type	T_* (kK)	$T_{2/3}$ (kK)	$\log(L/\mathrm{L_\odot})$	v_∞ ($\mathrm{km\,s^{-1}}$)	$\log \dot{M}$ ($\mathrm{M_\odot\,yr^{-1}}$)	$\dot{M}/\sqrt{f}$ ($10^{-5}\,\mathrm{M_\odot\,yr^{-1}}$)	C/He	O/He	$\log Q_{\mathrm{H^0}}$ ($\mathrm{s^{-1}}$)	$\log Q_{\mathrm{He^0}}$ ($\mathrm{s^{-1}}$)	$M_{\mathrm{v}}^{\mathrm{WC}}$ (mag)
11	WC8+O7.5 III	57	51	5.0	1550	−5.1	2.9	0.15	0.03	48.8	47.8	−3.7
90	WC7	71	29	5.5	2045	−4.6	8.0	0.25	0.03	49.3	48.7	−4.7
111	WC5	91	30	5.3	2300	−4.8	4.7	0.4	0.10	49.2	48.5	−4.2
135	WC8	63	27	5.2	1400	−4.9	3.8	0.13	0.03	49.1	48.3	−4.3
146	WC5+O8	57	33	5.7	2700	−4.5	10.5	0.08	0.02	49.6	48.7	−5.3

6 SUMMARY OF SPECTROSCOPIC RESULTS

In this section we discuss the results of our quantitative analyses, and make comparisons with previous studies.

6.1 Stellar parameters of WC stars

In Table 5, we provide a summary of the derived properties of our programme WC stars, including results for WR 11 and WR 111 from De Marco et al. (2000) and Hillier & Miller (1999), obtained using identical techniques. Despite our sample spanning WC5 to WC8, there is no obvious trend between spectral type and stellar temperature. Indeed, the WC5 component of WR 146 is found to have the lowest stellar temperature, although this is certainly a most unusual WCE star! The subtle behaviour of C III 5696 Å and C IV 5808 Å from our modelling indicates that, unfortunately, we are unable to use these as probes of wind ionization for WC5–8 stars (while we cannot obtain a simultaneous fit to both lines, a relatively small change in parameters can lead to a fit of either line).

Similarly, although there is considerable spread in carbon abundances, WR 146 exhibits the lowest carbon mass fraction, in

Table 6. Comparison of our derived stellar parameters for WR 135 with Howarth & Schmutz (1992; HS92) and Koesterke & Hamann (1995; KH95). We have adjusted their parameters to our assumed visual absolute magnitude ($M_v = -4.3$ mag).

Ref.	Model	$\log(L/L_\odot)$	T_* (kK)	v_∞ (km s^{-1})	$\dot{M}/\sqrt{f}$ ($M_\odot$ yr^{-1})	C/He
HS92	He	4.9	(35)	1500	5×10^{-5}	–
KH95	He+C	5.1	76	1300	6×10^{-5}	0.14
This work	He+C+O+Fe	5.2	63	1400	4×10^{-5}	0.13

contrast to the predicted increase in C/He ratio at earlier spectral type. Koesterke & Hamann (1995) derived a broad range of C/He ratios at each spectral type for WC5–8 stars.

How do the present line-blanketed, clumped results compare with previous studies? Unfortunately, WR 135 is the sole programme star that has been the subject of quantitative studies in the past. Eenens & Williams (1992) derived elemental abundances from IR recombination lines, estimating C/He = 0.12 by number, in excellent agreement with our determination of 0.13. Howarth & Schmutz (1992) used a pure helium non-LTE model analysis to investigate WR 135 based solely on 1-μm spectroscopy. Since pure helium models are expected to be inadequate for WC analyses, Koesterke & Hamann (1995) considered both carbon and helium in their study of WC stars, including WR 135.

In Table 6 we compare results from our present analysis of WR 135 with these previous studies, scaling their results to our absolute visual magnitude. Wind velocities and $\dot{M}/\sqrt{f}$ are in relatively good agreement, while the effect of including carbon and blanketing has a dramatic effect on the stellar temperatures and luminosities, such that the luminosity derived here is a factor of 2 times higher than Howarth & Schmutz (1992), who adopted a stellar temperature of 35 000 K.

Stellar parameters are in much better agreement with Koesterke & Hamann (1995). They compared specific line strengths with model grids at fixed C/He ratio, and chose simple model atoms of He I–II and C II–IV. Although spectral comparisons between model predictions and observations were not presented by Koesterke & Hamann (1995), the fit quality was judged to be poor, with large discrepancies for the C III λλ5696 and 6740 lines. Therefore, we have greater confidence in our results since detailed UV, optical and IR synthetic spectrophotometry compare favourably with observations.

From Table 6, blanketing and clumping conspire to revise the wind performance number, $(\dot{M}v_\infty)/(L/c)$, from 30 in the study of Koesterke & Hamann (1995) to just 5 for WR 135! For the entire sample, performance numbers are ⩽10, with previous studies indicating values of up to 100 (Howarth & Schmutz 1992; Koesterke & Hamann 1995).

6.2 Evolutionary status

The wide range in stellar luminosity of our sample of WC stars, $L/L_\odot = 10^5$ to $10^{5.7}$, implies a considerable range in current stellar masses. Following the mass–luminosity relation for hydrogen-free WR stars of Schaerer & Maeder (1992), present masses of 9 $M_\odot$ (WR 135), 13 $M_\odot$ (WR 90) and 19 $M_\odot$ (WR 146) are implied. In contrast, initial mass estimates are much more dependent on specific evolutionary tracks.

All models predict stars to pass through the WC phase at ages between 2.7 and 4.5 Myr. For initial 40 and 60 $M_\odot$ models, stellar masses during the early WC phase are predicted to be ∼14 $M_\odot$ and ∼24 $M_\odot$, respectively. At higher initial mass, the situation is

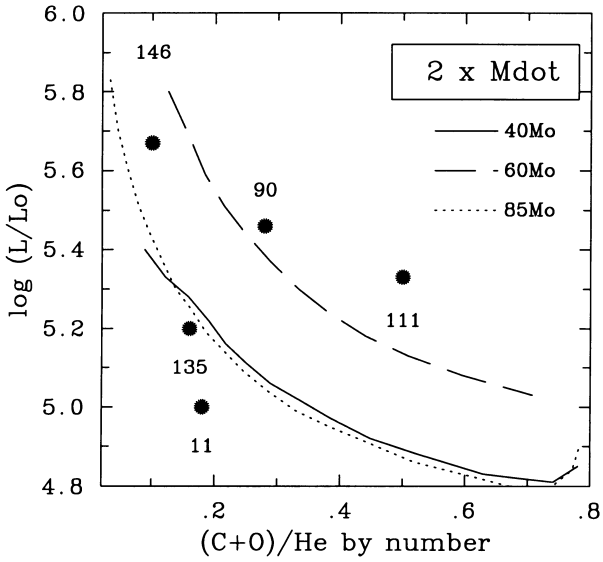

Figure 5. Comparison of measured (C + O)/He ratios versus luminosities for our programme stars, including WR 111 (WC5) from Hillier & Miller (1999), with theoretical expectations from the solar metallicity evolutionary tracks assuming enhanced (2×) mass loss (Meynet et al. 1994).

extremely model-dependent. For example, an evolutionary model with initial mass 120 $M_\odot$ will produce a 60 $M_\odot$ WC star using standard mass-loss rates of de Jager, Nieuwenhuijzen & van der Hucht (1988). Alternatively, a 10 $M_\odot$ WC star will result based on (2×) enhanced mass loss for the post-main-sequence and WNL phases (Schaller et al. 1992), or only a 4 $M_\odot$ WC star for (2×) enhanced mass loss during the entire stellar evolution (Meynet et al. 1994). Therefore, the present masses and ages of our programme WC stars are well constrained, but initial masses are not.

In order to attempt estimates of initial masses, we compare our derived (C+O)/He ratios versus stellar luminosities with evolutionary predictions in Fig. 5. Predictions for 40–120 $M_\odot$ initial models assume (2×) enhanced mass loss relative to de Jager et al. (1988) during the entire stellar evolution (Meynet et al. 1994). These models favour 60 $M_\odot$ for WR 146 and WR 90 and 40 $M_\odot$ *or* 85 $M_\odot$ for WR 135. Consequently, multiple initial mass estimates may result for individual stars. Nevertheless, we currently favour 40 $M_\odot$ for WR 135 and 60 $M_\odot$ for WR 146 and WR 90.

Specific comparisons between the stellar properties of WR 90, WR 135 and WR 146 and Meynet et al. (1994) evolutionary predictions are made in Table 7. Both the initial 60 $M_\odot$ and 85 $M_\odot$ models adopt mass-loss rates that exceed observations by large factors during early WC stages. This is because evolutionary models for hydrogen-free WR stars adopt mass-loss rates that are solely functions of mass (Langer 1989). Clearly, future evolutionary models should make allowance for more appropriate WR mass-loss rates.

Table 7. Comparison between our derived stellar parameters for WC stars and evolutionary predictions from Meynet et al. (1994).

WR	M ($M_\odot$)	τ (Myr)	T_* (kK)	$\log(L/L_\odot)$	$\dot{M}$ ($M_\odot\,yr^{-1}$)	C/He	O/He
90			71	5.5	2.5×10^{-5}	0.25	0.03
135			63	5.2	1.2×10^{-5}	0.13	0.03
146			57	5.7	3.3×10^{-5}	0.08	0.02
				$M_{init}=40\,M_\odot$			
	13	4.56	126	5.4	5.5×10^{-5}	0.08	0.004
	8	4.72	122	5.1	1.8×10^{-5}	0.25	0.04
				$M_{init}=60\,M_\odot$			
	23	3.57	136	5.8	24.6×10^{-5}	0.12	0.01
	12	3.67	131	5.4	4.8×10^{-5}	0.25	0.04
				$M_{init}=85\,M_\odot$			
	15	3.10	128	5.5	9.1×10^{-5}	0.07	0.004
	8	3.30	120	5.0	1.7×10^{-5}	0.25	0.04

Table 8. Comparison between predicted and observed 6-cm (4.9-GHz) radio fluxes in our programme stars, assuming $f=0.1$ for the UV/optical line-forming region. The filling factor entry in the table corresponds to the adopted value in the radio region, indicating the change in that quantity required to recover the observed flux at 4.9 GHz. We have included WR 11 in this table, since a neon abundance determination for this star is to be carried out in Section 7.2.

WR	Ionization state			T_e (kK)	f radio	$S_\nu^{6\,cm}$ (mJy) Pred.	Obs. (ref.)
11	He^+	C^{2+}	O^{2+}	8	0.10	20.5	
	He^+	C^{2+}	O^{2+}	8	0.05	32.5	32.2 (a)
	He^+	C^{2+}	O^+	8	0.10	20.2	
	He^+	C^+	O^+	8	0.10	15.1	
90	He^+	C^{2+}	O^{2+}	8	0.10	1.72	
	He^+	C^{2+}	O^{2+}	8	0.20	1.08	1.10 (b)
	He^+	C^{2+}	O^+	8	0.10	1.64	
	He^+	C^+	O^+	8	0.10	1.10	
135	He^+	C^{2+}	O^{2+}	8	0.10	0.54	0.60 (a)
	He^+	C^{2+}	O^+	8	0.10	0.51	
	He^+	C^+	O^+	8	0.10	0.40	
146	He^+	C^{2+}	O^{2+}	9	0.10	2.04	2.00 (c)
	He^+	C^{2+}	O^{2+}	9	0.20	1.29	
	He^+	C^{2+}	O^{2+}	9	0.30	0.98	
	He^+	C^{2+}	O^+	9	0.10	1.95	
	He^+	C^+	O^+	9	0.10	1.65	

Refs: (a) Leitherer et al. (1997); (b) Abbott et al. (1986); (c) Dougherty et al. (2000).

6.3 Radio fluxes

We now compare predicted radio fluxes from our spectroscopic mass-loss rates. Hillier & Miller (1999) provide a formulation based on equation (9) in Wright & Barlow (1975), allowing for the filling factor according to Abbott, Bieging & Churchwell (1981).

In all cases, the dominant ionization at the outer boundary of our models, $N_e\sim10^8\,cm^{-3}$ or $200R_*$ is He^+, C^{2+} and O^{2+} (see Fig. 3). Since the radio-emitting region lies at lower densities, we also consider cases in which C^+ and/or O^+ are dominant. Outer wind electron temperatures are typically 8000 K (Fig. 3), except for WR 146, for which the lower cooling produced by less metals implies 9000 K.

We compare predicted radio fluxes with observed values taken from the literature in Table 8, in which a uniform UV/optical filling factor of $f=0.1$ has been adopted throughout. Note that the quoted radio flux for WR 146 refers solely to the WC component (the southern mean emitted flux S_5 in Dougherty et al. 2000). We find that consistency is excellent for WR 135 and WR 146 for doubly ionized carbon and oxygen, while singly ionized carbon and oxygen are favoured for WR 90. However, C^+ is not predicted to be the dominant ionization stage in the outer wind of these stars (Fig. 3), so that the predicted radio flux for this star appears to be too high.

It is possible that the filling factors in the radio and optical forming regions differ significantly. The predicted radio flux of WR 90 would be in excellent agreement with the observed value if the radio filling factor was ~0.2, while that of WR 11 requires ~0.05. Hillier & Miller (1999) found a similar discrepancy in their study of WR 111. Note also that there is observational evidence that WR 90 may not be single, since it is a non-thermal emitter (Leitherer, Chapman & Koribalski 1997; Chapman et al. 1999).

We also include calculations for WR 11 in Table 8, since we attempt to rederive its neon abundance determination in Section 7. As for the other stars in our sample, possible variations in filling factor between the inner and outer wind are important.

7 NEON AND SULPHUR ABUNDANCES IN WC STARS

We are now in a position to determine neon abundances in our programme WC stars based on *ISO* spectroscopy, supplemented by sulphur determinations for WR 11. In this section we first provide a revised formulation for the determination of neon in a clumped medium, following BRA88, and subsequently provide measurements for each star.

7.1 Ionic abundances from fine-structure lines in an inhomogeneous wind

We have rederived the numerical and analytical forms for the determination of ionic abundances in clumped winds from BRA88. We consider a fine-structure line from ion i, with transition energy $h\nu_{ul}$. If D is the distance to the star and I_{ul} is the observed line flux, then

$$4\pi D^2 I_{ul}=\int_0^\infty n_u A_{ul} h\nu_{ul} 4\pi r^2 f\,dr\ erg\,s^{-1}, \quad (1)$$

where A_{ul} is the line transition probability and we have introduced the filling factor f into their formulation; n_u represents the density of ions in the upper level, and can be written as

$$n_u=f_u n_i\,cm^{-3}, \quad (2)$$

where n_i is the species ion density and f_u is the fractional population of the upper level. Upper level populations, f_u, were determined for each ion by solving the equations of statistical equilibrium using EQUIB (Adams & Howarth, private communication) for ⩾30 electron densities in the range 10^0 to $10^{12}\,cm^{-3}$, and nine electron temperatures covering 5 kK to 14 kK. Thus,

$$n_u=\frac{f_u\gamma_i A}{fr^2}\,cm^{-3}, \quad (3)$$

where γ_i is the fraction of all ions represented by ion species i,

$$\gamma_i = \frac{n_i}{\sum_j n_j}, \tag{4}$$

and A is the mass-loss parameter (equation 8 from BRA88). Combining equations (1)–(3), the filling factor term cancels out, leaving

$$I_{\rm ul} = \frac{\gamma_i}{D^2} A_{\rm ul} h\nu_{\rm ul} A \int_0^\infty f_{\rm u}(r,f,T)\,{\rm d}r \,{\rm erg\,cm^{-2}\,s^{-1}}. \tag{5}$$

We deviate from BRA88 by carrying out the integral in density, rather than radial, space. Since $r(N_{\rm e})$ is a bijection, we can modify this integral so that the dependence of $f_{\rm u}$ on A and f (and hence $\dot{M}$) is removed from the integral term. Equation (5) can then be modified to

$$\int_0^\infty f_{\rm u}(r,f,T)\,{\rm d}r = \sqrt{\frac{\gamma_{\rm e} A}{4f}} \int_0^\infty \frac{f_{\rm u}(N_{\rm e},T)}{N_{\rm e}^{1.5}}\,{\rm d}N_{\rm e}. \tag{6}$$

For a more straightforward numerical computation, equation (6) is slightly adjusted:

$$\int_0^\infty \frac{f_{\rm u}(N_{\rm e},T)}{N_{\rm e}^{1.5}}\,{\rm d}N_{\rm e} = \ln(10) \int_0^\infty \frac{f_{\rm u}(N_{\rm e},T)}{\sqrt{N_{\rm e}}}\,{\rm d}\log(N_{\rm e}). \tag{7}$$

The effect of this modification leads to a significant improvement over BRA88 who used an average value for each region Δr, since the line formation region is a very sensitive function of $f_{\rm u}$. Also, the dependence of the integral on $\dot{M}$ is removed. Consequently, BRA88 overestimated the integral term, producing a lower elemental abundance. Our final numerical expression for the ion number fraction γ_i is (cgs units)

$$\gamma_i = \frac{(4\pi\mu m_{\rm H} \upsilon_\infty)^{1.5}}{\ln(10) f^{0.25}} \left(\frac{\sqrt{f}}{\dot{M}}\right)^{1.5} \frac{1}{F_{\rm u}(T)} \frac{2D^2 I_{\rm ul}}{\sqrt{\gamma_{\rm e}} A_{\rm ul} h\nu_{\rm ul}}, \tag{8}$$

with

$$F_{\rm u}(T) = \int_0^\infty \frac{f_{\rm u}(N_{\rm e},T)}{\sqrt{N_{\rm e}}}\,{\rm d}\log(N_{\rm e}). \tag{9}$$

Provided radio and recombination processes are used to derive $\dot{M}/\sqrt{f}$, elemental abundances are only weakly dependent on the distance ($\propto D^{-0.25}$) since mass-loss rates depend on $D^{1.5}$. Therefore elemental abundances obtained with filling factors of $f = 0.1$ or 1.0 differ by a factor of 1.8.

In order to allow for the possibility of a clumped medium, the analytical expression for the ion number fraction given by BRA88 (their equation A13) also needs to be multiplied by a factor of $\sqrt{f}$. We include determinations of γ_i using both the integral and

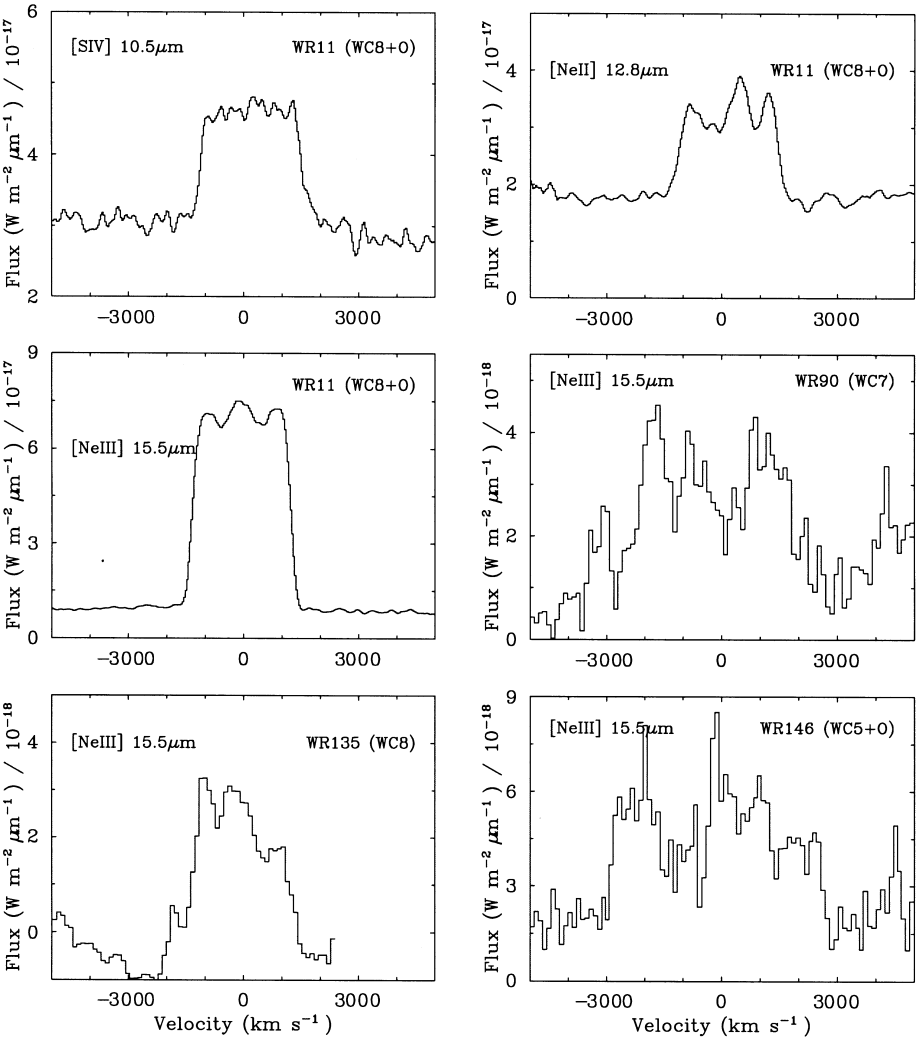

Figure 6. *ISO*-SWS observations of fine-structure [S IV] 10.5-μm, [Ne II] 12.8-μm and [Ne III] 15.5-μm emission in WR 11, WR 90, WR 135 and WR 146.

analytical expressions in our subsequent calculations. We find that the analytical expression is reliable to within ~20 per cent.

7.2 Neon abundances for WC stars

We are now in a position to evaluate neon abundances in our programme WC stars, using equation (8). Fig. 6 shows *ISO*-SWS observations of [Ne III] 15.55-μm emission for each of our programme stars, together with [Ne II] 12.8 μm in WR 11. Emission-line fluxes are listed in Table 9.

Table 9 also includes atomic quantities used to derive ion fractions. Transition probabilities are taken from the NIST Atomic Spectra Database, while collision strengths are obtained from papers in the IRON Project series (actual references are given in Table 9). *ISO* flux measurements for WR 11 compare closely with previous measurements from *IRAS* and ground-based observations (van der Hucht & Olnon (1985); BRA88), as indicated in Table 9.

In the following comparison, we include abundances derived from *ISO* mid-IR neon lines for WR 11, using stellar parameters derived by De Marco et al. (2000).

Neon abundance determinations are sensitive to the ionization balance in the line-forming region for the fine-structure lines, and is comparable to that of the radio forming continuum, $N_e \sim 10^5\,cm^{-3}$. Ne^+, with an ionization potential that is higher than C^+ and O^+, is observed solely in WR 11 (WC8). Therefore, we have allowed for the possibility that the carbon and oxygen ionization balances are singly ionized for WC8 stars, with He^+ and doubly ionized carbon and oxygen otherwise. Table 10 shows predicted ion abundances of Ne^{2+} for each case, plus measured Ne^+ for WR 11, with upper limits otherwise. In all cases $Ne/He \sim (3–4) \times 10^{-3}$ by number, significantly greater than the expected cosmic value of $Ne/He \sim 5 \times 10^{-4}$ in the C- and O-enriched WC environment.

It is possible that neon exists in (unseen) higher ionization stages, specifically Ne^{3+}. However, the ionization potential for Ne^{3+} (97 eV) is significantly higher than for C^{3+} (64 eV) and O^{3+} (77 eV), which are not expected to be present in the outer winds of WC stars (Fig. 3).

In summary, measurement of fine-structure lines of neon from *ISO*-SWS observations reveals $Ne/He = 0.003–0.004$ ($Ne/C \sim 0.02$), a factor of 6–8 times higher than cosmic abundances of $Ne/He = 0.0005$ for the carbon-rich winds of WC stars, supported also by sulphur abundance determinations. However, what additional sources of uncertainty are there in our Ne/He determinations, and why do our results for WR 11 differ from BRA88, who obtained $Ne/He = 0.001$?

Although the *ISO*-SWS neon line fluxes are in good agreement with the ground-based and *IRAS* neon line fluxes from BRA88 (Morris et al. 1998), we derive an elemental abundance that is *three* times higher. The source of this discrepancy is due to a different distance to WR 11, and to the use of a non-clumped mass-loss rate by BRA88. Morris et al. (2000) have recently emphasized the need for a reliable mass-loss rate estimate in the determination of neon abundances. In addition, our derived neon abundance is in good agreement with Morris et al. (1998), who combined *ISO*-SWS neon fluxes with the *Hipparcos* distance to WR 11, and the X-ray derived mass-loss rate of Stevens et al. (1996).

The other major factor affecting neon abundances is clumping. Our UV/optical analyses use filling factors of $f = 0.1$, yet we cannot observationally constrain the filling factor to better than $0.05 \leqslant f \leqslant 0.25$, indicating a further 20 per cent uncertainty in Ne/He. Of greater importance, we assume identical filling factors

Table 9. Observed mid-IR fine-structure line intensities (units of $10^{-12}\,erg\,cm^{-2}\,s^{-1}$), and adopted atomic parameters, including statistical weights of the upper and lower levels, ω_u and ω_l, transition probability A_{ul} and collision strength Ω_{ul} at $T_e = 8000$ K. Fluxes are obtained from *ISO*-SWS observations in all cases, except for literature measurements for WR 11, obtained from *IRAS*/LRS (van der Hucht & Olnon 1985) and the UCL spectrometer at the AAT (BRA88).

Ion	Transition	λ (μm)	ω_u	ω_l	A_{ul} (s^{-1})	Ref.	Ω_{ul} 8000 K	Ref.	WR 11 (WC8+O) *ISO*	WR 11 (WC8+O) IRAS/AAT	WR 90 *ISO* (WC7)	WR 135 *ISO* (WC8)	WR 146 *ISO* (WC5+O)
[S IV]	$^2P^o_{3/2}$–$^2P^o_{1/2}$	10.51	4	2	7.70×10^{-3}	a	8.47	c	15 ± 1*	19 ± 4	–	–	–
[Ne II]	$^2P^o_{3/2}$–$^2P^o_{1/2}$	12.81	2	4	8.59×10^{-3}	a	0.28	d	18 ± 1	17 ± 3	⩽1	⩽0.5	⩽1
[Ne III]	$^3P^o_1$–$^3P^o_2$	15.55	3	5	5.99×10^{-3}	a	0.76	e	82 ± 1	90 ± 20	6.5 ± 1	3.1 ± 0.2	9.4 ± 1
[S III]	$^3P^o_1$–$^3P^o_2$	18.68	5	3	2.07×10^{-3}	a	5.30	b	<1.8*	–	–	–	–

Refs: (a) Naqvi (1951); (b) Galavis, Mendoza & Zeippen (1995); (c) Saraph & Storey (1999); (d) Saraph & Tully (1994); (e) Butler & Zeippen (1994).
* [S III–IV] line fluxes are shown prior to correction for the presence of He I and C III stellar features (see text).

Table 10. Neon and sulphur abundances derived for the programme stars, using the stellar parameters given in the previous table. In all cases the ionization balance is assumed to consist of He^+, C^{2+} and O^{2+}. For each star, the first entry refers to the γ_i derived from the (more reliable) integration method, with the second obtained from the analytical expression.

WR	γ_e	Z	μ	$\gamma_{S^{2+}}$ (10^{-5})	$\gamma_{S^{3+}}$ (10^{-5})	S/He (10^{-5})	γ_{Ne^+} (10^{-4})	$\gamma_{Ne^{2+}}$ (10^{-4})	Ne/He (10^{-4})
11	1.137	1.189	5.14	1.9	3.1	5.9	5.4	21.6	31.9
				2.5	5.1	9.0	6.5	27.8	40.5
90	1.219	1.287	5.84	–	–	–	⩽4.0	22.6	⩽34.0
				–	–	–	⩽4.8	29.1	⩽43.4
135	1.138	1.189	5.21	–	–	–	⩽5.9	32.0	⩽44.0
				–	–	–	⩽7.0	41.1	⩽55.8
146	1.083	1.117	4.70	–	–	–	⩽2.8	22.8	⩽28.2
				–	–	–	⩽3.3	29.5	⩽36.1

for the optical line-forming region ($\approx 10^{11}\,\mathrm{cm}^{-3}$) and the neon emitting region ($\approx 10^{5}\,\mathrm{cm}^{-3}$). Neon abundances would be increased by 40 per cent for WR 90, decreased by 30 per cent for WR 11, with WR 146 and WR 135 unchanged, assuming that (i) UV/optical mass-loss rates are fully consistent with radio fluxes (recall Section 6.3), and that (ii) volume filling factors in the neon emitting region are identical to those in the radio region.

7.3 Sulphur abundances for WR 11

In order to assess the reliability of our derived abundances, we have also calculated the sulphur abundance for WR 11 based on *ISO* observations of fine-structure [S IV] 10.5-μm and [S III] 18.7-μm lines (Table 9). Since sulphur is not enhanced by nucleosynthesis, abundances should correspond to the cosmic value. The line-forming region for the sulphur fine-structure lines peaks at $N_e \sim 10^4\,\mathrm{cm}^{-3}$, somewhat lower than the neon lines.

ISO spectroscopy of [S IV] 10.5 μm confirms the line flux measured from ground-based spectroscopy by BRA88, while stellar modelling anticipates weak contamination from lines of He I (12–8) 10.52 μm and C III (20–17) 10.54 μm. The stellar analysis of WR 11 by De Marco et al. (2000) predicts a 15 per cent contribution from these lines to the observed flux, which has been corrected accordingly. For the first time in a Wolf–Rayet star, *ISO* reveals the presence of [S III] 18.7 μm, blended with the stellar He I (14–10) 18.62-μm feature, resulting in a 30 per cent decrease in [S III] flux. Use of an inappropriate mass-loss rate and distance for WR 11 led BRA88 to suggest $S^{3+}/He = 2.5 \times 10^{-5}$, such that they were obliged to predict $S^{2+} > S^{3+}$, with an expected high [S III] 18.7-μm line flux that is not confirmed by *ISO* observations.

From Table 10, we find $\gamma_{S^{2+}} = 1.9 \times 10^{-5}$ and $\gamma_{S^{3+}} = 3.1 \times 10^{-5}$, which imply $S/He = 6 \times 10^{-5}$ by number. This is in good agreement with the cosmic value of 7.5×10^{-5} for the C- and He-enriched environment of WR 11. Therefore, our determinations imply Ne/S = 50 for WR 11, a factor of 8 times greater than the cosmic value of Ne/S ~ 7. Since these lines are formed in similar

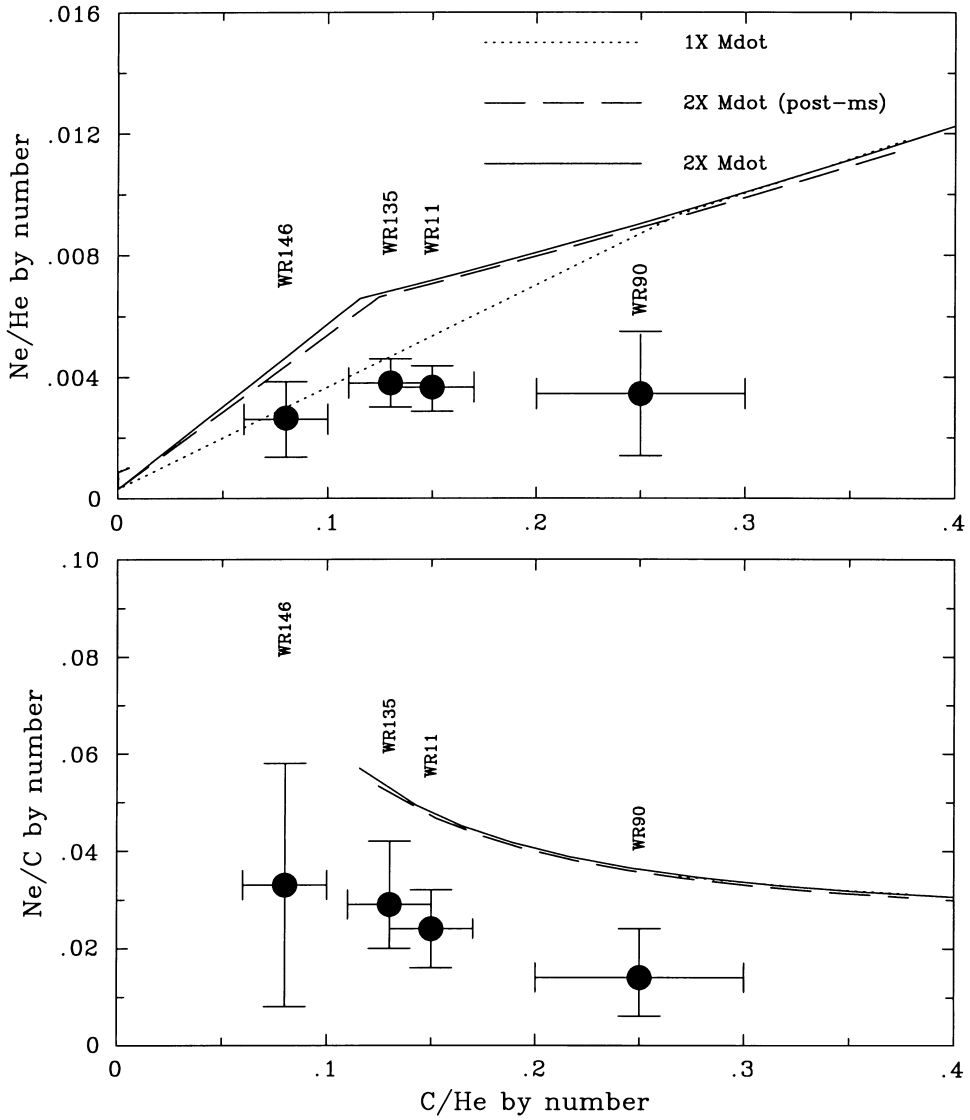

Figure 7. Comparison between Ne/C (bottom) and Ne/He (top) ratios versus measured C/He, also confronted with theoretical expectations from the solar metallicity evolutionary tracks of Schaller et al. (1992) and Meynet et al. (1994) for 60 $M_\odot$. Three tracks are shown: (i) normal mass-loss rates during the entire evolution of the star (dotted); (ii) enhanced (2×) mass loss during the post-main-sequence phase (dashed); (iii) enhanced (2×) mass loss during the entire stellar evolution (solid). Error bars account for uncertainties in distance and filling factor (see text).

regions of the stellar wind, Ne/S abundances are essentially independent of clumping, and reveal a degree of neon enrichment relative to sulphur that is equivalent to that derived earlier for He.

7.4 Comparison of abundances with theoretical predictions

Regarding theoretical expectations, the level of neon enrichment is expected to be strongly correlated with the carbon content (Schaller et al. 1992; Meynet et al. 1994). In Fig. 7 we compare observed Ne/He and Ne/C versus C/He ratios with theoretical expectations from the Schaller et al. (1992) and Meynet et al. (1994) evolutionary models at solar metallicity for an initial mass of $60\,M_{\odot}$. We find that observed neon abundances are a factor of 2 below expectations. Specifically, we derive $Ne/C = 0.02 \pm 0.01$ in all cases, while $Ne/C \geqslant 0.03$ is predicted during this phase of the WC evolution. Error bars shown in the figure account for uncertainties in distance and (uniform) filling factors, but do not allow for the possibility of a varying volume filling factor between the neon and UV/optical line-forming regions, which could be responsible for the discrepant cases.

8 SUMMARY

We have performed quantitative analyses of a small sample of WC5–8 stars, using models that account for line blanketing and clumping. Comparisons between synthetic spectra and dereddened UV to mid-IR observations are excellent, with few modelling deficiencies identified. Stellar parameters support previous determinations (e.g. Koesterke & Hamann 1995), except that the incorporation of blanketing yields higher stellar luminosities, while clumping indicates lower wind performance numbers, supporting the conclusions of Hillier & Miller (1999) for WR 111 (WC5). Future studies will derive properties of WC-type stars, at both earlier (WO) and later (WC9) spectral type, and investigate whether predicted ionizing properties are consistent with nebular observations (e.g. Crowther et al. 1999).

ISO-SWS spectroscopy reveals the presence of neon fine-structure transitions, allowing abundance determinations. Using a revised formulation of the BRA88 technique to account for wind clumping, we derive neon abundances of $Ne/He = (3\text{–}4) \times 10^{-3}$ by number, seven times higher than the cosmic value adjusted for the H-depleted WC environment, supported by $Ne/S = 50$ for WR 11 from sulphur fine-structure lines. The Ne enrichment is a factor of $\sim$2 times lower than predictions of current theoretical models. However, differences in volume filling factors between the (high-density) UV/optical line formation regions and (low-density) mid-IR fine-structure forming regions represent the greatest source of uncertainty in current Ne/He abundance determinations. Nevertheless, Ne/S provides an independent confirmation of the neon enrichment since it is *independent* of outer wind filling factors. Future large ground and space-based telescopes that are optimized for the IR will allow neon and sulphur line flux measurements and abundance determinations for more distant Wolf–Rayet stars. Of particularly interest are abundances in carbon- and oxygen-rich WO stars.

ACKNOWLEDGMENTS

This work is based on observations with *ISO*, an ESA project with instruments funded by ESA Member States (especially the PI countries: France, Germany, The Netherlands and the United Kingdom) with the participation of ISAS and NASA. Theoretical predictions presented here were possible only as a result of the Opacity Project, led by Professor Michael Seaton. Thanks are due to Dr Tim Harries for observing WR 90 on our behalf at the AAT. LD would like to acknowledge financial support from the UCL Perren Fund. PAC acknowledges financial support from a Royal Society University Research Fellowship. DJH gratefully acknowledges support by NASA through grant number NAG5-8211. The Anglo-Australian Telescope, Isaac Newton Telescope and UK Infrared Telescope are operated by the Anglo-Australian Observatory, Isaac Newton Group and Joint Astronomy Centre, respectively, on behalf of the Particle Physics and Astronomy Research Council.

REFERENCES

Abbott D. C., Bieging J. H., Churchwell E., 1981, ApJ, 250, 645
Abbott D. C., Bieging J. H., Churchwell E., Torres A. V., 1986, ApJ, 303, 239
Barlow M. J., Roche P. F., Aitken D. A., 1988, MNRAS, 232, 821 (BRA88)
Becker S. R., Butler K., 1992, A&A, 265, 647
Becker S. R., Butler K., 1995a, A&A, 294, 215
Becker S. R., Butler K., 1995b, A&A, 301, 187
Butler K., Zeippen C. J., 1994, A&AS, 108, 1
Cardelli J. A., Clayton G. C., Mathis J. S., 1989, ApJ, 345, 245
Chapman J., Leitherer C., Koribalski B., Bouter R., Storey M., 1999, ApJ, 518, 890
Conti P. S., Alschuler W. R., 1971, ApJ, 170, 325
Crowther P. A., Bohannan B., 1997, A&A, 317, 532
Crowther P. A., De Marco O., Barlow M. J., 1998, MNRAS, 296, 367
Crowther P. A., Pasquali A., De Marco O., Schmutz W., Hillier D. J., de Koter A., 1999, A&A, 350, 1007
Daly P. N., Beard S. M., 1992, SUN 27 (Rutherford Appleton Laboratory)
de Graauw Th. et al., 1996, A&A, 315, L49
de Jager C., Nieuwenhuijzen H., van der Hucht K. A., 1988, A&AS, 72, 259
De Marco O., Schmutz W., Crowther P. A., Hillier D. J., Dessart L., de Koter A., Schweickhardt J., 2000, A&A, in press
Dougherty S. M., Williams P. M., van der Hucht K. A., Bode M. F., Davis R. J., 1996, MNRAS, 280, 963
Dougherty S. M., Williams P. M., Pollacco D. L., 2000, MNRAS, in press
Eenens P. R. J., Williams P. M., 1992, MNRAS, 255, 227
Eenens P. R. J., Williams P. M., Wade R., 1991, MNRAS, 252, 300
Fernley J. A., Seaton M. J., Taylor K. T., 1987, J. Phys. B, 20, 6457
Galavis M. E., Mendoza C., Zeippen C. J., 1995, A&AS, 111, 347
Hillier D. J., 1987, ApJS, 68, 947
Hillier D. J., 1990, A&A, 231, 111
Hillier D. J., 1991, A&A, 247, 455
Hillier D. J., 1996, in Vreux J. M., Detal A., Fraipont-Caro D., Gosset E., Rauw G., eds, Proc. 33rd Liège Int. Astron. Colloq., Wolf–Rayet Stars in the Framework of Stellar Evolution. Univ. Liège, p. 509
Hillier D. J., Miller D. L., 1998, ApJ, 496, 407
Hillier D. J., Miller D. L., 1999, ApJ, 519, 354
Howarth I. D., 1983, MNRAS, 203, 301
Howarth I. D., Phillips A. P., 1986, MNRAS, 222, 809
Howarth I. D., Schmutz W., 1992, A&A, 261, 503
Howarth I. D., Murray J., Mills D., Berry D. S., 1998, SUN 50.21 (Rutherford Appleton Laboratory)
Kessler M. et al., 1996, A&A, 315, L27
Koesterke L., Hamann W.-R., 1995, A&A, 299, 503
Kurucz R. L., 1991, in Philip A. G. D., Upgren A. R., Janes K. A., eds, Precision Photometry: Astrophysics of the Galaxy. L. Davis Press, Schenectady, p. 27
Langer N., 1989, A&A, 220, 135
Leitherer C., Chapman J. M., Koribalski B., 1997, ApJ, 481, 898

Lepine S., Moffat A. F. J., 1999, ApJ, 514, 909
Lundström I., Stenholm B., 1984, A&AS, 58, 163
Luo D., Pradhan A. K., 1989, J. Phys. B, 22, 3377
Luo D., Pradhan A. K., Saraph H. E., Storey P. J., Yu Yan, 1989, J. Phys. B, 22, 389
Massey P., 1984, ApJ, 281, 789
Meynet G., Maeder A., Schaller G., Schaerer D., Charbonnel C., 1994, A&AS, 103, 97
Moffat A. F. J., 1999, in van der Hucht K. A., Koenigsberger G., Eenens P. R., eds, Proc. IAU Symp. 193, Wolf–Rayet Phenomena in Massive Stars and Starburst Galaxies. Astron. Soc. Pac., San Francisco, p. 278
Moffat A. F. J., Drissen L., Lamontagne R., Robert C., 1988, ApJ, 334, 1038
Morris P. W., Brownsberger K. R., Conti P. S., Massey P., Vacca W. D., 1993, ApJ, 412, 324
Morris P. W., van der Hucht K. A., Willis A. J., Williams P. M., 1998, Ap&SS, 255, 157
Morris P. W., van der Hucht K. A., Crowther P. A., Dessart L., Willis A. J., Williams P. M., 2000, A&A, 353, 624
Naqvi A. M., 1951, Thesis, Harvard Univ.
Niemela V., Shara M. M., Wallace D. J., Zurek D. R., Moffat A. F. J., 1998, AJ, 115, 2047
Nussbaumer H., Storey P. J., 1983, A&A, 126, 75
Nussbaumer H., Storey P. J., 1984, A&AS, 56, 293
Peach G., Saraph H. E., Seaton M. J., 1988, J. Phys. B, 21, 3669
Prinja R. K., Barlow M. J., Howarth I. D., 1990, ApJ, 361, 607
St Louis N., 1990, PhD thesis, Univ. London
St Louis N., Willis A. J., Stevens I. R., 1993, ApJ, 415, 298
Saraph H. E., Storey P. J., 1999, A&AS, 134, 369
Saraph H. E., Tully J. A., 1994, A&AS, 107, 29
Schaerer D., Maeder A., 1992, A&A, 263, 129
Schaerer D., Schmutz W., Grenon M., 1997, ApJ, 484, L153
Schaller G., Schaerer D., Meynet G., Maeder A., 1992, A&AS, 96, 269
Schmutz W., 1997, A&A, 321, 268
Schmutz W., Vacca W. D., 1991, A&AS, 89, 259
Seaton M. J., 1987, J. Phys. B, 20, 6363
Seaton M. J., 1995, The Opacity Project, Vol. 1. Institute of Physics, Bristol
Shortridge K. et al., 1999, SUN 86.17 (Rutherford Appleton Laboratory)
Smith L. F., 1968, MNRAS, 140, 409
Smith L. F., Shara M. M., Moffat A. F. J., 1990, ApJ, 358, 229
Steenman H., Thé P. S., 1989, Ap&SS, 159, 189
Steenman H., Thé P. S., 1991, Ap&SS, 184, 9
Stevens I. R., Corcoran M. F., Willis A. J., Skinner S. L., Pollock A. M. T., Nagase F., Koyama K., 1996, MNRAS, 283, 589
Torres-Dodgen A. V., Massey P., 1988, AJ, 96, 1076
Torres-Dodgen A. V., Carroll M., Tapia M., 1991, MNRAS, 249, 1
Tully J. A., Seaton M. J., Berrington K. A., 1990, J. Phys. B, 23, 3811
van der Hucht K. A., Olnon F. M., 1985, A&A, 149, 17
van der Hucht K. A., Conti P. S., Lundström I., Stenholm B., 1981, Space Sci. Rev., 28, 227
van der Hucht K. A., Hidayat B., Admiranto A. G., Supelli K. R., Doom C., 1988, A&A, 199, 217
van der Hucht K. A. et al., 1996, A&A, 315, L193
van der Hucht K. A. et al., 1997, New Astron., 2, 245
Wiese W. L., Smith M. W., Glennon B. M., 1966, Atomic Transition Probabilities, Vol. I, Hydrogen Through Neon. NSRDS-NDS 4
Willis A. J., van der Hucht K. A., Garmany C. D., Conti P. S., 1986, A&AS, 63, 417
Willis A. J., Dessart L., Crowther P. A., Morris P. W., Maeder A., Conti P. S., van der Hucht K. A., 1997, MNRAS, 290, 371 (Paper I)
Wright A. E., Barlow M. J., 1975, MNRAS, 170, 41
Yu Yan, Seaton M. J., 1987, J. Phys. B, 20, 6409
Yu Yan, Taylor K. T., Seaton M. J., 1987, J. Phys. B, 20, 6399

This paper has been typeset from a TEX/LATEX file prepared by the author.